NASA Technical Memorandum 86848



# Design and Performance Analysis of an Aeromaneuvering Orbital-Transfer Vehicle Concept

Gene P. Menees



October 1985

National Aeronautics and
Space Administration

NASA Technical Memorandum 86848

# Design and Performance Analysis of an Aeromaneuvering Orbital-Transfer Vehicle Concept

Gene P. Menees, Ames Research Center, Moffett Field, California

October 1985

National Aeronautics and
Space Administration

**Ames Research Center**
Moffett Field, California 94035

# DESIGN AND PERFORMANCE ANALYSIS OF AN AEROMANEUVERING ORBITAL-TRANSFER VEHICLE CONCEPT

Gene P. Menees*

NASA Ames Research Center
Moffett Field, CA 94035 - USA

## ABSTRACT

Systems requirements for design-optimized, lateral-turn performance were determined for reusable, space-based applications and low-Earth orbits involving large multiple plane-inclination changes. The aerothermodynamic analysis is the most advanced available for rarefied-hypersonic flow over lifting surfaces at incidence. The effects of leading-edge bluntness, low-density viscous phenomena, and finite-rate flow-field chemistry and surface catalysis are accounted for. The predicted aerothermal heating characteristics are correlated with thermal-control and flight-performance capabilities. The mission payload capacity for delivery, retrieval, and combined operations was determined for round-trip sorties extending to polar orbits. Recommendations are given for future design refinements. The results help to identify technology issues required to develop prototype operational vehicles.

## NOMENCLATURE

$C_A$ = atom mass fraction

$C_D$ = drag coefficient

$C_h$ = heat transfer coefficient

H = altitude

$K_r^2$ = Cheng's rarefaction parameter (Cheng, 1961)

$K_w$ = surface catalytic recombination rate

L/D = lift-to-drag ratio

$\dot{q}$ = convective heat flux

Q = total heat load over flight trajectory

$R_b$ = blunt leading-edge radius

t = flight time from H = 150 km

T = temperature

V = flight velocity

x,y,z = cartesian coordinates

$\alpha$ = angle of attack (referenced to aft-cone axis for bent biconic)

$\Delta$ = shock stand-off distance

$\Delta i$ = change in orbital inclination from Shuttle orbit (28.5°)

$\Delta V$ = propulsive thrust increment

---

*Research Scientist; Member AIAA; Associate Editor, AIAA Journal of Spacecraft and Rockets.

$\gamma$ = flight path angle relative to local horizon

$\Gamma$ = stability parameter (negative ratio of pitching moment and lift coefficients)

$\phi$ = bank angle of lift plane vector

Subscripts

cp = center of pressure location

e = boundary-layer edge or atmospheric entry condition at H = 150 km

f = atmospheric exit condition at H = 150 km

g = glide path angle

le = leading edge

min = minimum $\alpha$ to house transport complex

q = equivalent (referenced to leading-edge normal vector)

s = stagnation point

v = vibrational

## INTRODUCTION

In conceptual studies extending over the past two decades (Walberg, 1985; Menees, 1985a, 1985b) the potential of aeroassisted technology for enhancing orbital operations and planetary missions has been widely recognized. This technique calls for using the aerodynamic forces produced by grazing passes through the upper atmosphere to achieve the transition to local orbit by deceleration or directional change; earlier methods relied exclusively on propulsion power. The propellant saved by eliminating the costly propulsive maneuvers not only makes possible missions that are otherwise impractical but also substantially increases payload capability.

Exploratory studies (Menees, 1985b) have indicated that two classes of aeroassisted orbital-transfer vehicles (AOTVs) can satisfy a broad range of Earth-centered space transport missions. One design is useful primarily as a space freighter for transporting large payloads when time is not a constraint in the mission requirements. This "aerobraking" vehicle performs its orbit-change maneuvers by aerodynamic drag in the far-outer extent of the atmosphere to alleviate surface heat fluxes and pressure forces, which minimizes weight penalties for the aeroassist apparatus. An extensive design and mission-performance analysis for operations encompassing cislunar space was given previously (Menees, 1985c, 1985d; Davies, 1985a) for an AOTV design in this category.

The other generic AOTV design is a very high-lift "aeromaneuvering" vehicle. This is an essential operational requirement if time-constrained, aeroassisted maneuvers are to be accomplished between low-Earth orbits (LEOs) involving large, multiple plane-inclination changes. Such high-lift vehicles serve as space taxis. They achieve rapid response from one orbital plane to another but have the inherent liability of small payload fraction because of low volumetric efficiency. A typical mission scenario for an aeromaneuvering AOTV is illustrated in Fig. 1 (Davies, 1985a). The sequence of events for a Shuttle compatible vehicle consist of the following: 1) deploying the AOTV from the Shuttle cargo bay with the external fuel tanks attached; 2) igniting the rocket engines and descending toward Earth's atmosphere; 3) jettisoning the empty fuel tanks and entering the atmosphere; 4) banking and turning into a new orbit using the AOTV's aeromaneuvering capability; 5) exiting the atmosphere and rendezvousing with another orbiting body (e.g., a communications satellite).

Results were given previously (Menees, 1985d, 1985e; Davies, 1985a, 1985b; Brown, 1985) of a detailed systems design study for a configuration in the high-lift AOTV category. This work was the first to address the problem of rarefied-hypersonic flow over a lifting surface at incidence with the inclusion of appropriate viscous/inviscid interaction phenomena. The present work brings together into a coordinated whole the diverse details of the research activities at NASA Ames Research Center for high-lift AOTVs. Special emphasis is given to the problems of hypervelocity, low-density, viscous effects on flow-field dynamics and thermochemical relaxation effects.

## FLOW PHENOMENOLOGY

The principal features of the shock-layer physics that characterize aeromaneuvering AOTVs are illustrated in Fig. 2 (Menees, 1985e). Bow-shock waves are highly swept and relatively weak, since designs are by necessity slender to obtain high lift-drag ratios (L/D). Flow regimes are hypervelocity and low in density, with entry velocities that are typically of the order of 10 km/sec. These conditions produce flow-field temperatures that are sufficiently high to dissociate and ionize air species, but below the level for significant radiation transport. However, nonequilibrium relaxation phenomena may have important consequences to the shock-layer thermochemistry and transport properties. Finite-rate molecular diffusion and chemical reactions have a large variation in the rarefied-AOTV flight regimes. This variation can signifiantly affect surface catalysis and convective heating, which is especially important since convection is the dominant surface-heating mechanism. For low altitude flight regimes, turbulent boundary-layer transition criteria and hypersonic viscous/inviscid interaction effects become important factors in the flow-field analysis. However, the present study is concerned with transatmospheric trajectories which are sufficiently high that analysis based on Shuttle flight data indicates that laminar flow conditions prevail.

## VEHICLE DESIGN

The basic geometry of the present high-lift aeromaneuvering configuration is shown in Fig. 3 (Menees, 1985e). The design is completed by the addition of a transport complex to the upper surface that contains components for the propulsion system, command-control capsule (including avionics and reaction-control system motors for attitude control), and cargo module. The vehicle is approximately 35 m in length, which is necessary to accommodate the rocket engines and obtain the high-lift requirements for large payloads. The shape is derived from hypersonic lifting-body theory using truncated biconics with smoothing through the juncture point between the fore and aft cones to eliminate the discontinuity. The design avoids the complex shock-interaction effects of winged configurations, which cause highly localized heat fluxes and severe thermal control requirements. The aerodynamic characteristics are optimized in parametric studies by varying the angles of the fore and aft cones, the bend angle between the cones, and the upper-surface curvature, which is truncated with second-order polynomials. The results have been compared with traditional hypersonic lifting configurations and the advantages that provide design superiority identified, as will be discussed below. Complete details of the optimization procedure for the aerodynamic and vehicle-systems designs are given by Davies and Park (1985b).

## AERODYNAMIC CHARACTERISTICS

The lift, drag, and pitching-moment characteristics were determined from hypersonic Newtonian theory with appropriate corrections for low-density, viscous phenomena. The two-dimensional, boundary-layer, momentum equation (Schlictling, 1968) was used as the basis to account for surface curvature effects. The equations describing the boundary-layer growth rate (Wallace, 1965; Boettcher, 1965) were generated from the phenomena characteristic of rarefied-hypersonic flow over a flat plate. The model (McCroskey, 1966) of the various flow regimes (i.e., free-molecular at the leading edge evolving downstream through a transition region and merged layer before attaining the classical boundary-layer with weak interaction effects) is illustrated in Fig. 4.

Predictions for typical flight conditions are correlated in Fig. 5 (Menees, 1985b) as a function of altitude. The dramatic deterioration of lifting capability caused by the low-density viscous effects significantly decreases lateral-turn performance. Nevertheless, the L/D exceeds two over a broad altitude range. The necessity of operating the vehicle at the highest possible L/D to optimize the plane-change procedure and payload capacity is evident. The major constraint, however, is the altitude limitation imposed by thermal-control and materials technology, as will be discussed subsequently.

The effects of leading-edge bluntness were also determined because of the reusable, space-based operational requirements. Depending on the construction materials, gradual blunting or contouring of the leading edges may occur because of the accumulative heating effects of repeated flights. The bluntness is approximated in the analysis by circular cylinders superimposed along the leading edge. Typical results are given in Fig. 6 (Davies, 1985b). In general, it was found that leading-edge radii of the order of 10 cm could be easily accommodated without serious degradation of the aerodynamic characteristics.

The present results have been compared with traditional hypersonic lifting configurations (e.g., delta wings and truncated cones) and the superior design features identified. The common constraint in the comparative analysis is that each vehicle must accommodate a given volume in its

dead-air region that is associated with transporting functions. This "transport complex" is sized to the Shuttle cargo bay and contains the vehicle's systems component. Results from optimization studies for the placement of the transport complex are given in Fig. 7 for typical flight conditions (Davies, 1985b). A comparison of L/D based on the payload constraints for $\alpha_q$ is given in Fig. 8, and the corresponding values of $\Gamma$ (which incorporate the variable $x_{cp}$ and static margin) are compared in Fig. 9 (Davies, 1985b). The results indicate that all three configurations provide similar values of L/D under the constraint of the given transport complex. The bent biconic, however, is the only design that provides longitudinal stability and self-trimming capability over a broad $\alpha$ range. This design feature results from the geometry of the vehicle and is very advantageous because of the large magnitudes of the stabilizing forces.

## TRAJECTORY ANALYSIS

The principal flight parameters ($V$, $\gamma$, $\phi$) were varied in parametric comparative studies to determine the relative trade-offs between plane-change capability and the corresponding aerothermodynamic heating requirements (Menees, 1985e). The objective was to maintain the highest possible altitude to minimize the surface heating, yet still obtain substantial aeroturning ($\Delta i$) and the necessary aerobraking for optimal transfer to the target LEO. Only aerodynamic transatmospheric maneuvers are considered in this study. (The synergistic maneuver, or simultaneous application of propulsive thrust, will be analyzed in future work.) The flight strategy employed during the atmospheric pass consists of three phases: (1) the entry phase in which $V_e$, $\gamma_e$, and $\phi_e$ are selected to achieve a trajectory perigee that provides the desired compromise in $\Delta i$ and $\dot{q}_s$ ($\phi_e = 90°$); (2) the glide phase in which $\gamma_g$ and $\phi_g$ are held nearly constant to maintain high altitude [$\phi_g \approx 180°$ to produce negative lift, an aerodynamic strategy previously proposed (Menees, 1985c) to minimize surface heating and aerodynamic forces]; and (3) the exit phase in which $\gamma_f$ and $\phi_f$ are selected for maximum lateral turning ($\phi_f = 90°$) and optimal orbital transfer with minimal propulsion energy. Two iterations on $\gamma$ are required in the overall procedure. The first is at the transition from the entry to glide phases at the altitude where a force balance occurs, and the second at the transition from the glide to exit phases where $V_e$ is selected for tangential circularization at the target LEO. Representative results are given in Fig. 10 (Menees, 1985e) for entry velocities ranging from 9 to 11.5 km/s. Extending $V_e$ beyond this range produces marginal tradeoffs for $\Delta i$ and $\dot{q}_s$. The corresponding aeroturning or plane-inclination change characteristics of the vehicle are shown in Fig. 11. For geosynchronous orbit (GEO)-return entry conditions ($V_e \approx 10.3$ km/s), generally a standard comparative base, $\Delta i$ is about 32°, which provides a substantial capability.

## AEROTHERMODYNAMIC HEATING

The probability of finite blunting motivated the development of a new CFD (computational fluid dynamics) code (Brown, 1985) that predicts the convective heating to leading-edges of small radii in the highly energetic, rarefied-flow, flight regimes characteristic of aeromaneuvering AOTVs. These conditions produce unique flow phenomena that are without previous complete analysis. For example, the shock and boundary-layer thicknesses increase (see Fig. 12), and the flow develops from the "viscous-layer" type, through an "incipient merged layer," into a fully developed "merged" layer in which the shock and boundary layers cannot be considered separate (Probstein, 1960). In addition, finite-rate chemical and vibrational relaxation effects become dominant, since the post-shock flow is in a state of thermochemical nonequilibrium. The traditional Rankine-Hugoniot, shock-jump relations become invalid and must be modified to account for the viscous transport, or "shock-slip" conditions (Cheng, 1961; Park, 1985). The new viscous-shock-layer code incorporates all of the relevant physics of the flow phenomena except ionization, which will be included in future work. The unique contribution is the addition of thermal-nonequilibrium effects to the chemical relaxation solutions. The code is based on the thin-layer form of the boundary-layer equations for stagnation-point flow (Park, 1964). Although developed from continuum theory, this approach provides good results up to the free-molecular limit, with the low-density effects properly accounted for.

The impact of the two-temperature (T, Tv) gas model used herein for vibrational relaxation is illustrated in Fig. 13 (Brown, 1985). The vibrational temperature controls the molecular dissociation rate and, therefore, the concentration of species, which determines the diffusive portion of the convective heat transfer. The $\Delta$ for the $R_b = 20$ cm body is insufficient to allow $T_v$ and $T$ to equilibrate. Therefore, the $C_A$ profiles are vastly different between the thermal nonequilibrium and equilibrium cases. The corresponding effect on the convective heat transfer is shown in Fig. 14 (Brown, 1985) and the typical region of AOTV peak heating indicated. It should be noted that the benefits of noncatalytic surfaces are reduced by thermal nonequilibrium. This occurs because the reduced dissociation resulting from vibrational nonequilibrium provides a larger heat source to increase the surface heating.

Results that are typical of the predicted stagnation-point heat-flux distributions at the vehicle tip (centerline) are shown in Fig. 15 for the $V_e$ = 10.3 km/s trajectory. The calculations are based on $R_b$ = 10 cm and a surface temperature of 1500 K, which provides a $K_w$ of 5.7 m/s for the Shuttle-like ceramic material assumed for the vehicle surface (Scott, 1983). The low catalyticity of this material substantially reduces $\dot{q}_s$ (by as much as 40% over the later stages of the trajectory). The increase caused by vibrational nonequilibrium is significant and confined to the higher altitudes of the entry phase where rarefied effects are more pronounced.

Typical results for the heat-flux distribution around the leading edge of the vehicle are shown in Fig. 16 for the peak-heating point in the $V_e$ = 10.3 km/s trajectory. Two cases are given, which include the variation for both angle of attack and leading-edge sweep and for leading-edge sweep only. The stagnation-point heat-transfer calculations were obtained for hemispherical blunting of the vehicle tip, with the assumption that incidence effects were negligible. The swept-back leading edges, however, more closely approximate circular cylinders that are oblique to the flow, and neglecting incidence effects may be invalid. The results shown represent approximate upper and lower limits.

Representative streamwise distributions of the surface heat flux on the windward surface are shown in Fig. 17 (Menees, 1985e) for the three flight trajectories analyzed. The results correspond to two locations on the vehicle surface near the peak heating points: the centerline [Fig. 17(a)] and an outboard location at x = 9.0 m [Fig. 17(b) and Fig. 3]. The calculations were obtained using the weak-interaction effects formulation (McCroskey, 1966; Wallace, 1965) corrected for incidence, as being the most appropriate downstream match to the blunt leading-edge flow. The overall result is that the magnitude of $\dot{q}_s$ decreases very rapidly from the leading edge and is less than 20 W/cm$^2$ over most of the vehicle surface. Also shown in Fig. 17(a) is a predicted CFD, fully coupled, equilibrium solution for an equivalent 40°-sphere cone and $V_e$ ≈ 10.3 km/s (Menees, 1985c). The difference between this result and the present solution is about a factor of two, which is reasonable considering the physics involved. The CFD solution is axisymmetric and three dimensional, whereas the present flat-plate solution is two dimensional. This difference produces strong, viscous, cross-flow effects that increase the surface heating. Furthermore, the incidence angles for the two solutions differ (i.e., 45° for the CFD and about 30° for the present analysis), which causes additional increases that can easily account for the overall difference in the predictions.

## THERMAL CONTROL

The heat-shielding requirements of the vehicle were analyzed for the constraints imposed by reusable space-based applications. The leading-edge heating is the dominant factor in restricting the operational ceiling, since the heat transfer and loads over most of the surface are modest (<10 W/cm$^2$) for a broad altitude range. Existing techniques in which light-weight, aeroshell, structural designs are used for both hot and insulated applications can accommodate the thermal-protection requirements for all of the vehicle surface except the small localized region around the leading edge. Thermal-control materials and methods for cooling the leading edge must provide for toleration of the highest possible temperature, thus optimizing orbital change operations; therefore, their selection is critically important to high-lift AOTVs.

The results of initial screening studies to identify candidate leading-edge materials is summarized in Fig. 18 (Menees, 1985d, 1985e, 1985f). Although incomplete, this work may be useful in guiding future efforts. The range of application of the various materials is indicated for upper temperature limits based on the mass loss for a 1 mm thick shield and twenty-five flights of 300 s duration. In addition to high melting temperatures, the key factors influencing the selection of materials are low oxidation and vaporization properties in an oxygen environment. The geometry of the lifting surface is also a factor; however, strength and thermal-shock effects are not critical issues because the aerodynamic loads are moderate. The practical near-future limit (≈ two years development time) will probably be provided by a fibrous-reusable-ceramic-insulation material (FRCI) being developed at NASA Ames Research Center for space applications. This material has a surface temperature and radiative heat transfer capability of about 2500 K and 130 W/cm$^2$, respectively.

Other strategies that may alleviate the constraints imposed by reusable materials include the use of high-temperature ablators or forced and active cooling techniques that use the propulsion fuel or other fluids. For example, Salkeld (1981) has proposed a system, transpiration cooled with water, that protects a reusable all-metal spacecraft flying a hot reentry corridor, with descent from GEO. Calculated skin temperatures range above 4000 K for the stagnation point to nearly 1400 K on the underside. However, there are serious compromises to consider for the payload sacrificed as a result of the volume and weight penalties necessary to implement active cooling requirements. Another possible solution to the leading-edge problem is to replace

the affected areas between missions with new materials, since the severe heat transfer occurs only in small localized regions.

The essential surface heating requirements are summarized in Fig. 19 and correlated with aeromaneuvering plane-change and thermal-control capabilities. The limitations imposed by the near-future development of high-temperature, reusable materials (e.g., FRCI) and active cooling techniques are noted on the figure for equilibrium radiative emission of all the absorbed heat. The ceramics severely constrain the aeroturning capability; however, transpiration cooling dramatically improves $\Delta i$ to make values as much as 45° possible. The $Q_s$ for these flight conditions is high (about that for the Galileo probe), which is caused by the long duration of the atmospheric pass. These results do not, however, account for the reduction in $Q_s$ due to conduction and radiative emission, which may also be substantial because of the long flight time before rendevouz with the target orbit.

## MISSION PERFORMANCE ANALYSIS

An essential aspect of this work is a detailed analysis of the proposed high-lift AOTV's ability to satisfy specified mission requirements for payload delivery, retrieval, and combined delivery/retrieval operations. Studies were conducted for a broad range of LEO sortie missions extending to polar orbits. Both the base and target orbits had fixed altitudes of 400 km, with the inclination of the base orbit being equivalent to that of the Shuttle orbit (28.5°). This procedure is considered to be an average of proposed LEO sortie operations that involve both multiple-plane and moderate-altitude orbital changes. Altitude differences of approximately $10^4$ km can be accommodated by small changes in the aeroassist maneuver without significant propellant penalties. The calculations were made using the vehicle-weight specifications given in Table 1, the full detials of which were given previously (Menees, 1985c). For space-based operations, it is proposed to deploy the vehicle, without propellant, in several sections and assemble the components in space. Because of the high circular velocities of LEOs and the limitations of the vehicle's L/D characteristics, a propulsive strategy involving three burns is used as an adjunct to aerodynamic lift to enhance orbital-change maneuvers. This technique is illustrated in Fig. 20 (Menees, 1985c, 1985e) and basically involves transfer orbits of high eccentricity and apogee. Part of the plane change is accomplished propulsively at a much greater altitude than the target LEO, with low expenditure of propellant because of the reduced circular velocity.

The payload capacity for round-trip sorties involving plane changes of about 60°, 75°, and 90° (i.e., $\Delta i$ = 31°, 45°, and 61.5°) is illustrated in Figs. 21(a), (b), and (c), respectively (Menees, 1985e). The analysis is based on the plane-change capability for $V_e$ = 10.3 km/s and the normal-growth technology of liquid rocket engines having a specific impulse of 480 s. Generous allowances are included for propellant losses resulting from gruidance-navigation-control corrections, docking maneuvers, and boil off over the duration of the mission. The optimum orbital-change maneuver is to achieve all of the specified plane changes aerodynamically by direct decircularization from the base LEO. However, this maneuver is generally impractical because of the reduced aerodynamic-lift capability imposed by the relatively low-entry velocity. The various orbital-change strategies that are compared in the present study are listed in Table 2.

The all-propulsive direct maneuver of Case 1 cannot achieve any payload capability. Employing the three-impulse, propulsive-thrust maneuver with the transfer-orbit apogee at GEO provides moderate payload capability for $\Delta i$ = 31° and small payload capability for $\Delta i$ = 45°. The application of the vehicle's aeromaneuvering capability in combination with the three-impulse-thrust maneuver produces dramatic increases and is the only method that achieves payload for the polar orbit. However, Cases 2 and 3 require sacrifices in the mission duration. The time for the roundtrip scenario is about 21 hr, since the GEO distance is traversed twice. If rapid-response, time-constrained requirements are a factor, then the direct maneuver of Case 4 provides the best alternative for payload capability. This maneuver requires raising the entry velocity to the equivalent GEO-return value by a propulsive boost performed in conjunction with the GEO-decircularization burn. For the polar mission, it may also be possible to achieve payload by the synergistic technique or flight trajectories that plunge deeper into the lower atmosphere to increase the aerodynamic lift and plane-change capability. However, these methods must be compromised by increased aerothermodynamic-heating requirements.

## CONCLUDING REMARKS

A comprehensive study has been conducted that establishes the approximate aerothermodynamic and thermal-control requirements of a proposed high-lift AOTV design for LEO sortie missions involving large-multiple, plane-inclination changes. The aerodynamic characteristics are the first to account for hypervelocity, low-density, viscous phenomena. The surface heating predictions are

the most advanced developed and include finite-rate thermochemical effects on both the flow field and surface catalysis.

The flight strategy used for the aeroassist maneuver is designed to achieve an acceptable compromise between the surface-heating characteristics and aeromaneuvering capability. Severe heat transfer, beyond the range of contemporary reusable thermal-protection materials, occurs only in highly localized regions around the leading edge. However, total heat loads are substantial because of the long duration of the atmospheric transits. Ablating materials or active-cooling techniques are required to accommodate the heating requirements necessary to achieve significant plane-inclination changes (e.g., transpiration cooling may make possible aeromaneuvering plane changes as great as 45°). The mission performance with realistic aeromaneuvering capability for payload delivery and retrieval is demonstrated for LEO sorties extending to polar orbits. Substantial capacity is obtained for all scenarios with proper application of the three-impulse, propulsive-thrust, orbital-change maneuver. No payload is currently possible for rapid-response, time-constrained polar missions; however, improved lifting capability obtained by reducing the vehicle's transport complex requirements may achieve some small payload delivery.

Future design optimization requires advancements in the aerodynamic/aerothermodynamic prediction methods that account for rarefaction phenomena and real-gas effects. A multidimensional CFD code must incorporate these features, since the three-dimensional surface contour produces nontrivial effects. In addition, there are important thermochemical problems that must be addressed. Principal among these are nonequilibrium reaction rates and transport properties, which have wide but unknown variations in the rarefied-AOTV flight regimes and significantly affect surface catalysis and convective heating.

## REFERENCES


Boettcher, R. D., G. Koppenwaller, and H. Legge (1965). Flat-plate skin friction in the range between continuum and free-molecular flow. Rarefied Gas Dynamics, Part 1, 51, pp. 349-359.

Brown, K. G. (1985). Chemical and thermal nonequilibrium heat transfer analysis for hypervelocity low Reynolds number flow. AIAA Paper 1033.

Cheng, H. K. (1962). Hypersonic shock-layer theory of the stagnation region at low Reynolds number. Proceedings of the 1961 Heat Transfer and Fluid Mechanics Institute, Stanford University Press, Stanford, Calif., pp. 161-175.

Davies, C. B. and C. Park (1985a). Aerodynamics of generalized bent biconics for aeroassisted orbital-transfer vehicles. AIAA J. of Spacecraft and Rockets, 22, 104-111.

Davies, C. B. and C. Park (1985b). Optimum configuration of high-lift orbital-transfer vehicles. AIAA Paper 85-1059.

Kang, S. W. (1970). Nonequilibrium ionized hypersonic flow over a blunt body at low Reynolds number. AIAA J., 8, 1263-1270.

McCroskey, W. J., S. M. Bogdonoff, and J. G. McDougall (1966). An experimental model for the sharp flat plate in rarefied hypersonic flow. AIAA J., 4, 1580-1587.

Menees, G. P. (1985a). Trajectory analysis of radiative heating for planetary missions with aerobraking of spacecraft. AIAA J. of Spacecraft and Rockets, 22, 37-45.

Menees, G. P. (1985b). Thermal protection requirements for near-Earth aeroassisted orbital transfer missions. In H. F. Nelson (Ed.), Thermal Design of Aeroassisted Orbital Transfer Vehicles, AIAA Progress in Astronautics and Aeronautics, Vol. 96, pp. 257-285.

Menees, G. P., C. Park, and J. F. Wilson (1985c). Design and performance analysis of a conical aerobrake orbital transfer vehicle concept. In H. F. Nelson (Ed.), Thermal Design of Aeroassisted Orbital Transfer Vehicles, AIAA Progress in Astronautics and Aeronautics, Vol. 96, pp. 286-308.

Menees, G. P., C. B. Davies, J. F. Wilson, and K. G. Brown (1985d). Aerothermodynamic heating analysis of aerobraking and aeromaneuvering orbital transfer vehicles. In H. F. Nelson (Ed.), Thermal Design of Aeroassisted Orbital Transfer Vehicles, AIAA Progress in Astronautics and Aeronautics, Vol. 96, pp. 338-360.

Menees, G. P., K. G. Brown, J. F. Wilson, and C. B. Davies (1985e). Aerothermodynamic heating and performance analysis of a high-lift aeromaneuvering AOTV concept. AIAA Paper 85-1060.

Menees, G. P., C. Park, J. F. Wilson, and K. G. Brown (1985f). Determination of atmospheric density using a space launched projectile. AIAA Paper 85-0327.

Park, C. (1985). Problems of rate chemistry in the flight regimes of aeroassisted orbital transfer vehicles. In H. F. Nelson (Ed.), Thermal Design of Aeroassisted Orbital Transfer Vehicles, AIAA Progress in Astronautics and Aeronautics, Vol. 96, pp. 511-537.

Park, C. (1964). Dissociative relaxation in viscous hypersonic shock layers. AIAA J., 2, 511-537.

Probstein, R. F. and N. H. Kemp (1960). Viscous aerodynamic characteristics in hypersonic rarefied gas flow. AIAA J. of the Aero/Space Sciences, 27, 174-192.

Salkeld, R., R. Beichel, and R. Skulsky (1981). A reusable space vehicle for descent from high orbits. AIAA Astronautics and Aeronautics, 4, 46-63.
Schlictling, H. (1968). Boundary Layer Theory, 6th Ed., McGraw-Hill, New York.
Scott, C. D. (1983). Effects of nonequilibrium and catalysis on Shuttle heat transfer. AIAA Paper 83-1485.
Walberg, G. D. (1985). A survey of aeroassisted orbit transfer. AIAA J. of Spacecraft and Rockets, 22, 3-18.
Wallace, J. E. and A. F. Burke (1965). An experimental study of surface and flow field effects in hypersonic low density flow over a flat plate. Rarefied Gas Dynamics, Supplement 3, 1, 485-507.

TABLE 1. Vehicle Specifications for Mission Performance Analysis

| | |
|---|---|
| Gross (zero payload) weight | 23,822 kg |
| Nominal fuel weight (97% of total; i.e., 3% reserves) | 18,480 kg |
| Total allowed lift-off weight (gross weight + payload) | 29,484 kg |
| Dry weight of disposable external tank | 1,000 kg |
| Maximum fuel weight in disposable external tank | 4,662 kg |

TABLE 2. Orbital Change Strategies for Payload Calculations Involving Sorties between LEOs with Large Multiple Plane-Inclination Changes (480 s Specific Impulse Rocket Engine)

| | |
|---|---|
| Case 1 | All propulsive direct maneuver from base to target LEO |
| Case 2 | All propulsive maneuver using three-impulse thrust method for low eccentricity transfer orbit with apogee at GEO (21 hr roundtrip duration) |
| Case 3 | Combination aerodynamic and three-impusle thrust maneuver with $\Delta i$ required in excess of aeromaneuvering capability achieved propulsively at apogee of GEO transfer orbit (21 hr roundtrip duration) |
| Case 4 | Combination aerodynamic and propulsive direct maneuver by boosting down from LEO on equivalent GEO descent ellipse |

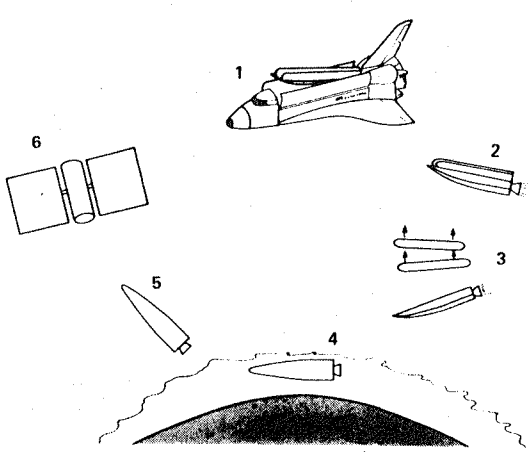


Fig. 1. Typical aeromaneuvering AOTV mission between Shuttle and satellite orbits.

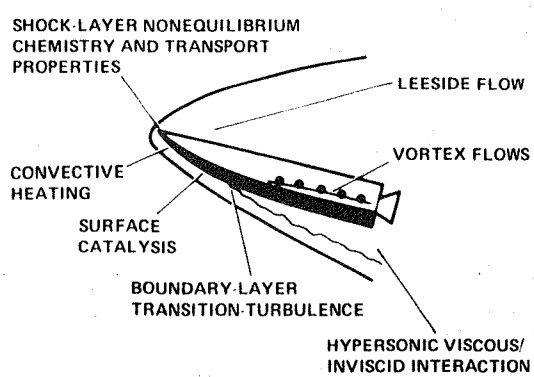


Fig. 2. Hypervelocity flow-field phenomenology of high-lift aeromaneuvering sortie vehicle.

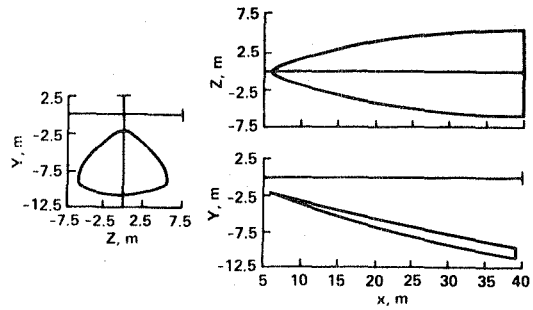


(a) TWO DIMENSIONAL

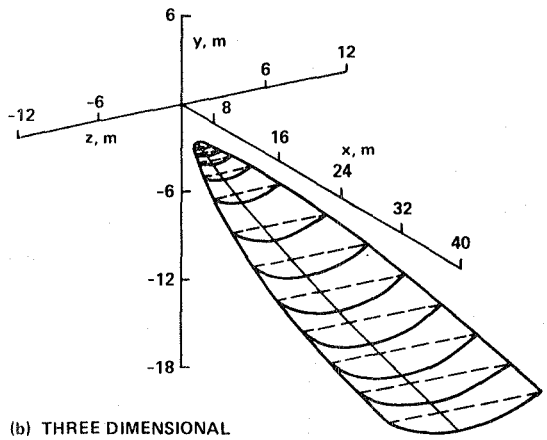


(b) THREE DIMENSIONAL

Fig. 3. Geometry of high-lift aeromaneuvering truncated, bent-biconic AOTV concept (fore-cone half angle = 20°; aft-cone half angle = 8°; bend angle = 2°).

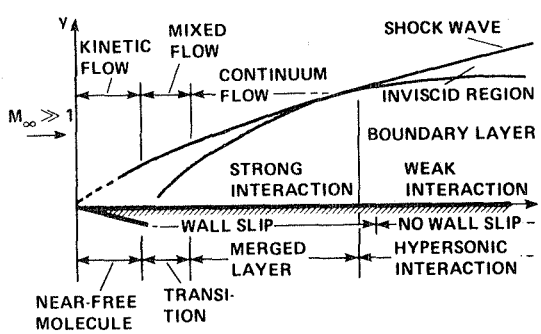


Fig. 4. Flow regimes in rarefied-hypersonic flow past a flat plate with sharp leading edges (McCroskey, 1966).

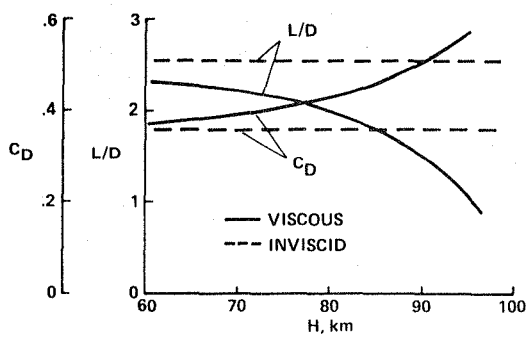


Fig. 5. Typical aerodynamic characteristics ($V_e$ = 10.3 km/s, $\alpha$ = 6.5°).

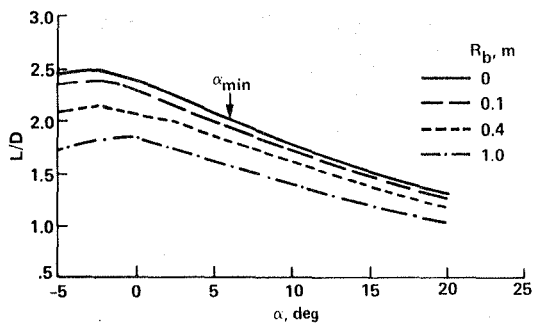


Fig. 6. Effect of leading-edge bluntness on L/D (H = 80 km, $V_e$ = 10.3 km/s, $\alpha$ = 6.5°).

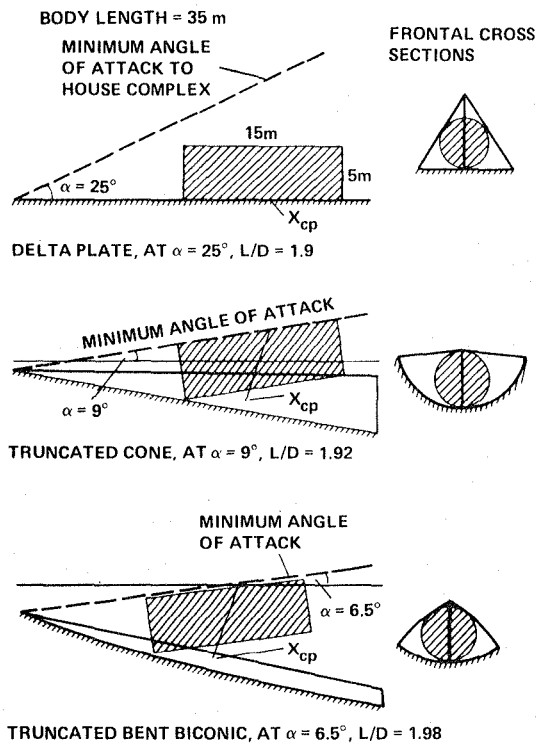


Fig. 7. Optimum placement of transport complex (H = 80 km, $V_e$ = 10.3 km/s).

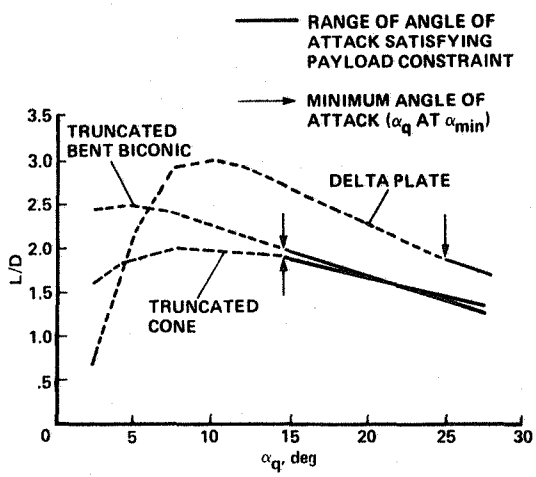


Fig. 8. Valid range of L/D based on payload constraints (H = 80 km, $V_e$ = 10.3 km/s).

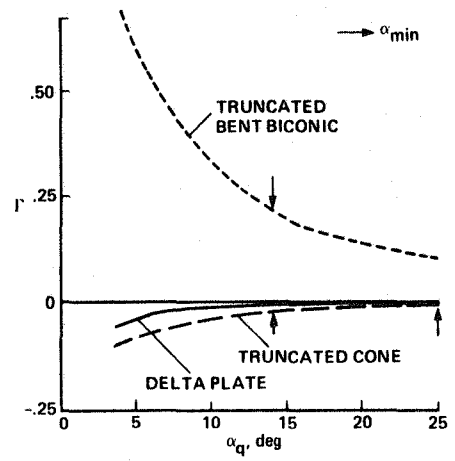


Fig. 9. Comparison of stability parameters (H = 80 km, $V_e$ = 10.3 km/s).

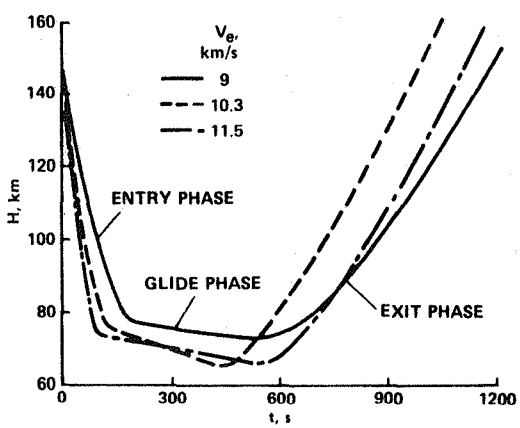


Fig. 10. Flight trajectories for various entry conditions and optimal orbital transfer to target LEO.

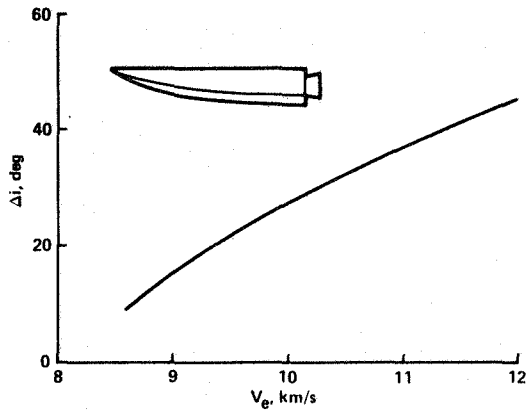


Fig. 11. Plane-inclination change capability as a function of entry velocity.

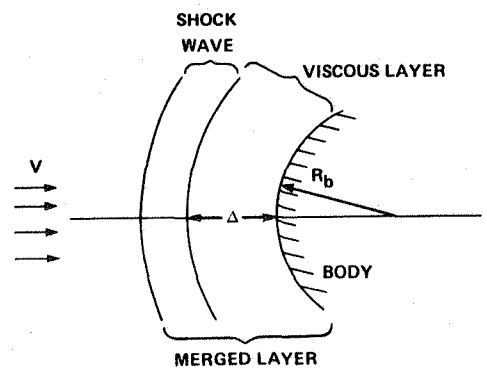


- VISCOUS LAYER: RANKINE-HUGONIOT SHOCK RELATIONS
- INCIPIENT MERGED LAYER: SHOCK-SLIP CONDITIONS
- FULLY MERGED LAYER: SOLVE THROUGH SHOCK

Fig. 12. Stagnation region model for hypersonic-rarefied flow.

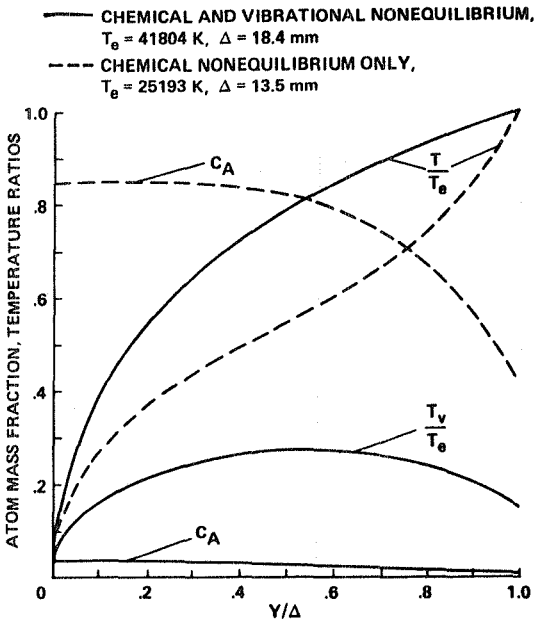


Fig. 13. Comparison of vibrational nonequilibrium and vibrational equilibrium solutions for a noncatalytic wall ($R_b$ = 20 cm, H = 80 km, V = 10 km/s).

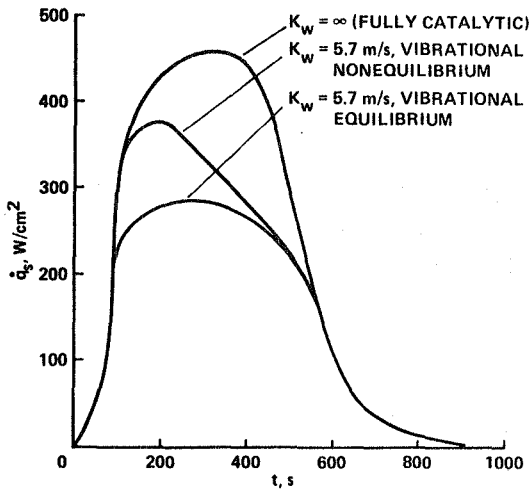


Fig. 15. Effect of vibrational nonequilibrium on stagnation-point heat-flux distribution over $V_e$ = 10.3 km/s flight trajectory (vehicle centerline).

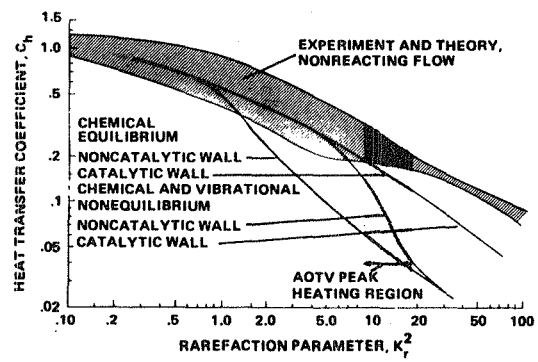


Fig. 14. Correlation of convective heat transfer rates.

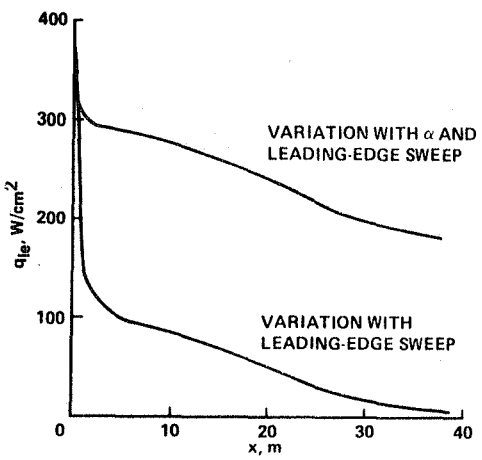


Fig. 16. Leading-edge heat-flux distributions at peak heating point in $V_e$ = 10.3 km/s trajectory.

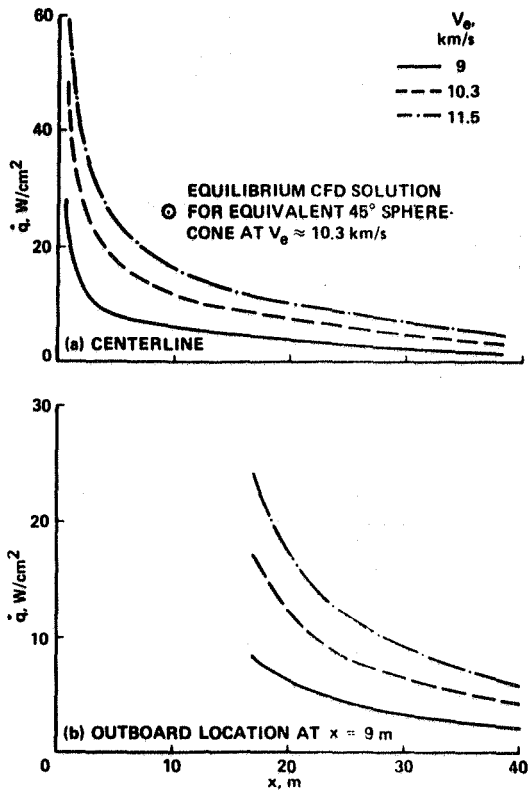


Fig. 17. Streamwise heat-flux distributions near peak heating point in flight trajectories.

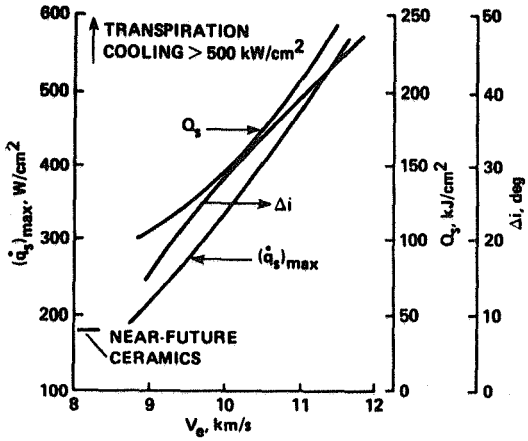


Fig. 19. Summary of maximum heating requirements and correlation with thermal-control capabilities.

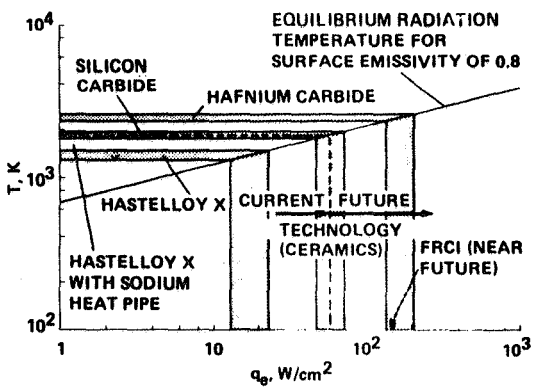


Fig. 18. Radiative heat-rejection characteristics of candidate leading-edge thermal-protection materials.

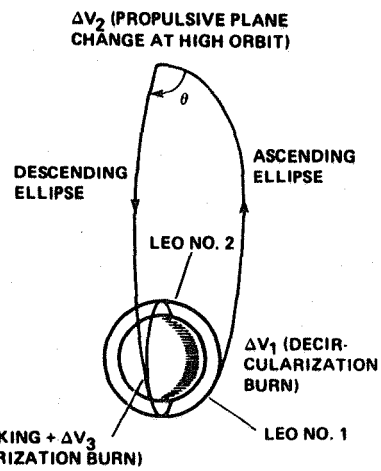


Fig. 20. Three-impulse, propulsive-thrust strategy to minimize propellant usage for sorties between LEOs requiring large plane changes.

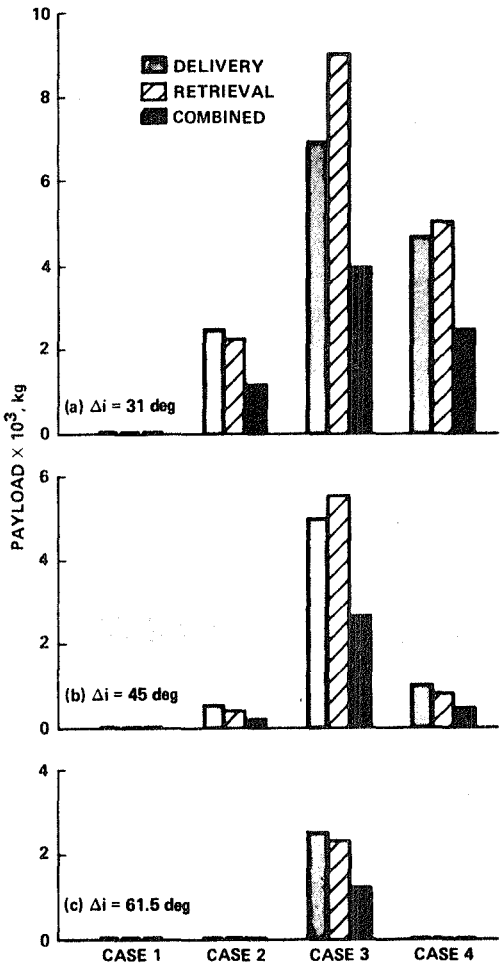


Fig. 21. Maximum payload capability for delivery, retrieval, and combined delivery/retrieval roundtrip sortie missions from LEO at H = 400 km.

| 1. Report No. | 2. Government Accession No. | 3. Recipient's Catalog No. |
|---|---|---|
| NASA TM-86848 | | |

| 4. Title and Subtitle | 5. Report Date |
|---|---|
| DESIGN AND PERFORMANCE ANALYSIS OF AN AERO-MANEUVERING ORBITAL-TRANSFER VEHICLE CONCEPT | October 1985 |
| | 6. Performing Organization Code |

| 7. Author(s) | 8. Performing Organization Report No. |
|---|---|
| Gene P. Menees | 85398 |
| | 10. Work Unit No. |

| 9. Performing Organization Name and Address | 11. Contract or Grant No. |
|---|---|
| Ames Research Center<br>Moffett Field, CA 94035 | |
| | 13. Type of Report and Period Covered |
| 12. Sponsoring Agency Name and Address | Technical Memorandum |
| National Aeronautics and Space Administration<br>Washington, DC 20546 | 14. Sponsoring Agency Code<br>505-35-11 |

15. Supplementary Notes

Point of Contact: Gene P. Menees, MS 230-3, Ames Research Center, Moffett Field, CA 94035, (415)694-6086 or FTS 464-6086

16. Abstract

Systems requirements for design-optimized, lateral-turn performance were determined for reusable, space-based applications and low-Earth orbits involving large multiple plane-inclination changes. The aerothermodynamic analysis is the most advanced available for rarefied-hypersonic flow over lifting surfaces at incidence. The effects of leading-edge bluntness, low-density viscous phenomena, and finite-rate flow-field chemistry and surface catalysis are accounted for. The predicted aerothermal heating characteristics are correlated with thermal-control and flight-performance capabilities. The mission payload capacity for delivery, retrieval, and combined operations was determined for round-trip sorties extending to polar orbits. Recommendations are given for future design refinements. The results help to identify technology issues required to develop prototype operational vehicles.

| 17. Key Words (Suggested by Author(s)) | 18. Distribution Statement |
|---|---|
| Spacecraft design | Unlimited<br><br>Subject Category - 18 |

| 19. Security Classif. (of this report) | 20. Security Classif. (of this page) | 21. No. of Pages | 22. Price* |
|---|---|---|---|
| Unclassified | Unclassified | 16 | |

*For sale by the National Technical Information Service, Springfield, Virginia 22161

End of Document